Published in final edited form as:
Cell Rep. 2014 June 26; 7(6): 2042–2053. doi:10.1016/j.celrep.2014.05.017.

Mitochondrial Pyruvate Carrier 2 Hypomorphism in Mice Leads to Defects in Glucose-Stimulated Insulin Secretion

Patrick A. Vigueira[#1], **Kyle S. McCommis**[#1], **George G. Schweitzer**[1], **Maria S. Remedi**[2], **Kari T. Chambers**[1], **Xiaorong Fu**[3], **William G. McDonald**[4], **Serena L. Cole**[4], **Jerry R. Colca**[4], **Rolf F. Kletzien**[4], **Shawn C. Burgess**[3], and **Brian N. Finck**[1]

[1]Division of Geriatrics and Nutritional Sciences, Department of Medicine, Washington University School of Medicine, St. Louis, MO 63110, USA

[2]Department of Cell Biology and Physiology, Washington University School of Medicine, St. Louis, MO 63110, USA

[3]Advanced Imaging Research Center and Department of Pharmacology, University of Texas Southwestern Medical Center, Dallas, TX 75390, USA

[4]Metabolic Solutions Development Company, Kalamazoo, MI 49007, USA

[#] These authors contributed equally to this work.

SUMMARY

Carrier-facilitated pyruvate transport across the inner mitochondrial membrane plays an essential role in anabolic and catabolic intermediary metabolism. The mitochondrial pyruvate carrier 2 (Mpc2) is believed to be a component of the complex that facilitates mitochondrial pyruvate import. Complete MPC2 deficiency resulted in embryonic lethality in mice. However, a second mouse line expressing an N-terminal truncated MPC2 protein ($Mpc2^{\Delta 16}$) was viable, but exhibited reduced capacity for mitochondrial pyruvate oxidation. Metabolic studies demonstrated exaggerated blood lactate concentrations after pyruvate, glucose, or insulin challenge in $Mpc2^{\Delta 16}$ mice. Additionally, compared to WT controls, $Mpc2^{\Delta 16}$ mice exhibited normal insulin sensitivity, but elevated blood glucose after bolus pyruvate or glucose injection. This was attributable to reduced glucose-stimulated insulin secretion and was corrected by sulfonylurea K_{ATP} channel inhibitor administration. Collectively, these data are consistent with a role for MPC2 in

Address correspondence to: Brian N. Finck, Washington University School of Medicine 660 S. Euclid Ave Box 8031 St. Louis, MO 63110, bfinck@wustl.edu, phone: 314-362-8963.

Author contributions: P.A.V. and K.S.M.: performed experiments, analyzed data, generated figures, and wrote the manuscript. G.G.S. and M.S.R.: performed experiments, analyzed data, generated figures, and wrote portions of the manuscript the manuscript. K.T.C. and X.F.: performed experiments and edited manuscript. W.G.M.: performed experiments, analyzed data, generated figures, and wrote portions of the manuscript the manuscript. S.L.C.: performed experiments and edited manuscript. J.R.C. and R.F.K.: analyzed data, and edited the manuscript the manuscript. S.C.B. and B.N.F.: analyzed data, and wrote portions of the manuscript the manuscript.

mitochondrial pyruvate import and suggest that Mpc2 deficiency results in defective pancreatic beta cell glucose sensing.

INTRODUCTION

Pyruvate is an important three-carbon intermediate in energy metabolism and is a central substrate in carbohydrate, fat, and amino acid catabolic and anabolic pathways. Pyruvate is generated in the cytoplasm through glycolysis and subsequently, is transported into the mitochondrion for oxidation or carboxylation, which is required for several critical metabolic processes (Figure 1A). For example, mitochondrial pyruvate carboxylation in the mitochondrial matrix results in the formation of oxaloacetate (an anaplerotic reaction) required for the biosynthesis of glucose via gluconeogenesis. Pyruvate entry into the mitochondrial matrix is also required for pyruvate oxidation, which is a prerequisite for the production of reducing equivalents in the TCA cycle and production of citrate for de novo lipogenesis. Both pyruvate oxidation and carboxylation are critical for glucose-stimulated insulin secretion (GSIS) in pancreatic beta cells (Jensen et al., 2008; Prentki et al., 2013; Sugden and Holness, 2011). Elevated blood glucose causes an increase in the intracellular ratio of ATP/ADP via increased mitochondrial pyruvate oxidation (Prentki et al., 2013; Sugden and Holness, 2011). ATP inhibits K_{ATP} channels leading to depolarization, Ca^{2+} influx, and the release of insulin into the circulation (Huopio et al., 2002). Anaplerotic mitochondrial pyruvate metabolism activates pyruvate cycling pathways that alter NADPH and regulates insulin secretion by inhibiting K_{ATP} channel activity as well (Jensen et al., 2008).

The existence of carrier-assisted transport of pyruvate across the inner mitochondrial membrane was demonstrated in the 1970's (Halestrap, 1975; Halestrap and Denton, 1975; Papa et al., 1971). However, the proteins that facilitate pyruvate import into the mitochondrial matrix have only recently been identified (Bricker et al., 2012; Herzig et al., 2012). New evidence has emerged that the mitochondrial pyruvate carrier (MPC) is composed of two proteins, MPC1 and MPC2, which form a hetero-oligomeric complex in the inner mitochondrial membrane and that both proteins are required for complex activity and stability (Bricker et al., 2012; Herzig et al., 2012). The MPC protein complex has been determined to be essential for mitochondrial pyruvate transport in *Drosophila* and yeast (Bricker et al., 2012; Herzig et al., 2012). In humans, mutations in MPC1 have been identified and associated with defects in mitochondrial pyruvate metabolism, lactic acidosis, hyperpyruvatemia, severe illness, and failure to thrive (Bricker et al., 2012; Brivet, 2003). Since its discovery, interest in the MPC complex as a drug target for cancer, neurological disorders, and metabolic diseases has been extremely high. Recent work suggests that insulin-sensitizing thiazolidinedione compounds bind the MPC complex (Colca et al., 2013) and modulate mitochondrial pyruvate oxidation (Divakaruni et al., 2013; Colca et al., 2013). Thus, a better understanding of MPC function has the potential to advance our knowledge of intermediary metabolism and impact drug discovery for current public health problems.

Herein, we report the generation and characterization of two MPC2-deficient mouse strains. Although complete MPC2 deficiency resulted in embryonic lethality, mice expressing a

truncated, partially-functional MPC2 protein were viable. Diminished pyruvate metabolism led to elevated blood lactate concentrations, particularly when mice were challenged with stimuli that increased glucose metabolism. The mutant mice also exhibited elevated blood glucose during glucose tolerance and pyruvate tolerance tests that was likely due to reduced GSIS. Additionally, glucose intolerance could be corrected by administration of K_{ATP} channel-inhibiting sulfonylurea drugs. These studies demonstrate the importance of mitochondrial pyruvate transport to glucose homeostasis in a mammalian system and support the continued exploration of mitochondrial function in complex metabolic diseases.

RESULTS

Tissue expression of MPC proteins

We first isolated various tissues from C57BL/6 mice to determine relative Mpc mRNA and MPC protein expression. We detected large variations in MPC protein (Figure 1B,C) and mRNA expression (Figure 1D) with the highest levels observed in tissues with greater mitochondrial abundance. Isolation and equal loading of mitochondrial lysate from these tissues somewhat normalized MPC1 and MPC2 protein expression (Supplemental Figure 1A,B). However, MPC protein was still most abundant in highly oxidative tissues even when corrected for mitochondrial protein content.

Generation of Mpc2-deficient mice

The Mpc2 allele was targeted for deletion by using zinc-finger nuclease technology. The first line of mice harbored a deletion of 2 nucleotides just downstream of the start codon (Supplemental Figure 2A), resulting in a frameshift mutation and likely complete loss of protein product ($Mpc2^{-/-}$ mice). The mutation results in embryonic lethality in homozygous embryos. However, the number of heterozygous mice present at weaning was as predicted by Mendelian ratios (p=0.717; Supplemental Table 1), and these mice were overtly indistinguishable from their WT littermates. Lethality in homozygous embryos likely occurs between embryonic days 11 and 13, a period when robust mitochondrial biogenesis takes place (Cámara et al., 2011; Larsson et al., 1998; Metodiev et al., 2009; Park et al., 2007). Timed mating studies yielded expected Mendelian ratios at embryonic days 10 and 11 (p=0.496; Supplemental Table 2), but no viable homozygote embryos at embryonic day 13 (Supplemental Table 3). Western blots of the tissues of heterozygous ($Mpc2^{+/-}$) mice demonstrated only a modest reduction in MPC2 and MPC1 protein compared to WT controls (Supplemental Figure 2B). Pyruvate-driven oxygen consumption by isolated mitochondria from $Mpc2^{+/-}$ mice was not diminished compared to WT mitochondria (Supplemental Figure 2C).

A second attempted knockout strategy resulted in the deletion of 20 nucleotides including the original start codon for MPC2 translation. Despite the deletion, Mpc2 mRNA was expressed at normal levels (data not shown) and MPC2 protein translation proceeded from a second downstream start codon (Supplemental Figure 2A). This resulted in a truncated protein that lacked the first 16 amino acids residues of the N-terminus ($MPC2^{\Delta 16}$). Pups homozygous for the truncated allele were born in expected Mendelian ratios (p=0.995; Supplemental Table 1) and were outwardly normal. The truncated protein, detected by

western blotting with an antibody against the C-terminus of MPC2, was less abundant than the WT protein in all tissues examined, except for BAT (Figure 2A). The $Mpc2^{\Delta 16}$ mutation led to a marked reduction in the abundance of MPC1 protein, likely reflecting the maintenance of a stoichiometric ratio of MPC1 and MPC2 protein in the complex. Immunoprecipitation studies also indicated that the $Mpc2^{\Delta 16}$ mutant protein co-immunoprecipitated less MPC1 protein, suggesting that the interaction between the two proteins is significantly weakened by the loss of these 16 amino acids of MPC2 (Figure 2B). Abundance of the pyruvate dehydrogenase (PDH) complex and pyruvate carboxylase (PC) proteins were not altered in various tissues of the $Mpc2^{\Delta 16}$ mice, suggesting a lack of significant downstream alterations in pyruvate metabolic enzymes (Figure 2A). Western blotting of subfractionated kidney and heart demonstrated that the truncated $Mpc2^{\Delta 16}$ protein properly localized to mitochondria (Figure 2C) and specifically to the inner mitochondrial membrane (Figure 2D).

Isolated $Mpc2^{\Delta 16}$ mitochondria have reduced oxygen consumption

$Mpc2^{\Delta 16}$ mice were healthy and appeared outwardly normal, suggesting that the MPC complex was at least partially functional. Plasma triglyceride was decreased, and plasma ketone concentrations were increased in $Mpc2^{\Delta 16}$ mice compared to WT control mice (Table 1), suggesting increased reliance on fat oxidation. Possibly consistent with a reduced capacity for mitochondrial pyruvate import, blood lactate concentrations were also significantly elevated (Table 1).

Therefore, we evaluated the effects of the MPC2 truncation on oxygen consumption in isolated mitochondria. We used heart and kidney tissue due to their high mitochondrial density and high MPC expression. $Mpc2^{\Delta 16}$ mitochondria from heart or kidney exhibited 25-30% lower rates of pyruvate/malate-stimulated respiration in DNP-uncoupled conditions compared to WT controls (Figure 3A). Addition of methyl-pyruvate, a membrane-permeable pyruvate analog, rescued oxygen consumption to WT levels in $Mpc2^{\Delta 16}$ mitochondria. Additionally, maximal oxygen consumption rates in $Mpc2^{\Delta 16}$ mitochondria with glutamate/malate or succinate/rotenone were unaltered compared to WT controls. Together these data suggest a specific effect of the $Mpc2^{\Delta 16}$ mutation on mitochondrial pyruvate oxidation.

Mitochondrial membrane potential is normal in fibroblasts from $Mpc2^{\Delta 16}$ mice

With the observed defect in pyruvate oxidation in $Mpc2^{\Delta 16}$ tissues, we investigated whether these mitochondria displayed any sign of overt dysfunction by assessing mitochondrial membrane potential ($\Delta\Psi_M$) in isolated adult fibroblasts of WT and $Mpc2^{\Delta 16}$ mice. TMRE staining revealed no difference in $\Delta\Psi_M$, a comprehensive measure of overall mitochondrial function, in $Mpc2^{\Delta 16}$ fibroblasts compared to WT controls (Figure 3B). The lack of effect on mitochondrial membrane potential was likely due to the small decrease in pyruvate-stimulated respiration and the maintained ability to metabolize other substrates.

Exercise endurance is normal in $Mpc2^{\Delta 16}$ mice

During exercise, significant quantities of pyruvate, which is interconverted to lactate, are generated via anaerobic glycolysis in skeletal muscle. Lactate, transported by the blood to the liver, is converted back to glucose that can again be used anaerobically as an energy

source in muscle. This process, known as the Cori cycle (Katz and Tayek, 1999; Pilkis et al., 1988), depends on pyruvate import in liver mitochondria. Therefore, we challenged $Mpc2^{\Delta 16}$ homozygote and $Mpc2^{+/-}$ mice using an acute endurance exercise bout of gradually increasing intensity until exhaustion (Figure 3C). The average blood glucose concentration of the $Mpc2^{\Delta 16}$ mice was not different from WT controls in the 60 minutes after exercise (Figure 3C). However, average blood lactate of the $Mpc2^{\Delta 16}$ was approximately two-fold higher compared to WT controls immediately after exercise and remained significantly elevated for 30 minutes post-exercise (Figure 3C). Post-exercise blood lactate and glucose concentrations were not different between $Mpc2^{+/-}$ and WT mice (Figure 3C). Despite the robust differences in blood lactate concentrations post-exercise, we observed no significant differences in acute endurance exercise capacity among the genotypes (Figure 3C).

Elevated blood glucose and lactate in $Mpc2^{\Delta 16}$ mice following pyruvate injection

To test the effects of the Mpc2 mutations on the ability to dispose of pyruvate in vivo, we subjected $Mpc2^{\Delta 16}$ homozygotes and $Mpc2^{+/-}$ mice to an intraperitoneal pyruvate tolerance test (PTT). Following pyruvate injection, blood lactate increased five-fold in all groups. However, the decline in blood lactate concentration was significantly slower in $Mpc2^{\Delta 16}$ mice compared to WT controls (Figure 4A). Blood glucose and lactate levels were not different between $Mpc2^{+/-}$ and WT mice. Compared to WT mice, $Mpc2^{\Delta 16}$ mice also exhibited a significantly greater blood glucose excursion (Figure 4A). These data are consistent with reduced pyruvate utilization resulting in elevated blood lactate concentrations.

To specifically evaluate the effect of the $Mpc2^{\Delta 16}$ mutation on pyruvate gluconeogenesis and other intracellular pathways of pyruvate metabolism, we repeated the pyruvate challenge in $Mpc2^{\Delta 16}$ mice with uniformly labeled [U-^{13}C]pyruvate. The mice were sacrificed, plasma and tissue were collected 60 minutes post-injection and fractional ^{13}C enrichments were evaluated by mass spectrometry. There were no differences in hepatic oxaloacetate, malate, or fumarate concentrations or enrichments (Supplemental Figure 3), indicating that liver mitochondrial pyruvate anaplerosis is intact in $Mpc2^{\Delta 16}$ mice. Although the fractional enrichment of plasma glucose was unaffected by the $Mpc2^{\Delta 16}$ mutation (Figure 4B), plasma glucose concentration, and therefore the total amount of ^{13}C-labeled plasma glucose was significantly elevated in $Mpc2^{\Delta 16}$ mice versus WT mice (Figure 4B). These data suggest that the capacity for pyruvate-derived gluconeogenesis is intact in $Mpc2^{\Delta 16}$ mice. Incorporation of ^{13}C-label into plasma lactate was not different between $Mpc2^{\Delta 16}$ and WT control groups (Figure 4C). However, due to increased lactate concentration in the blood, ^{13}C-labeled plasma lactate was significantly elevated in $Mpc2^{\Delta 16}$ mice compared to WT controls (Figure 4C), consistent with decreased mitochondrial pyruvate metabolism in extrahepatic tissues. Additionally, expression of liver gluconeogenic enzymes was unaltered in $Mpc2^{\Delta 16}$ mice except that Pck2, which encodes the mitochondrial form of phosphoenolpyruvate carboxykinase, was significantly decreased (Figure 4D), suggested that compensatory activation of these genes does not explain the intact gluconeogenic flux. Altogether, these data suggest that hepatic gluconeogenesis is not impaired in $Mpc2^{\Delta 16}$ mice.

Mpc2$^{\Delta 16}$ mice are sensitive to insulin, but have reduced plasma insulin and elevated blood glucose

One possible explanation for the elevated blood glucose concentration in PTT studies is that Mpc2$^{\Delta 16}$ mice are insulin-resistant. Insulin tolerance tests (ITT) were conducted to examine insulin effectiveness. Although blood lactate during the ITT was significantly elevated in Mpc2$^{\Delta 16}$ mice compared to WT mice, blood glucose concentrations at all time points and area under the curve (AUC) were not different, suggesting that insulin-stimulated glucose disposal is normal in Mpc2$^{\Delta 16}$ mice (Figure 5A). Insulin-stimulated phosphorylation of Akt in liver was significantly enhanced (Figure 5B) and was unaltered in gastroc muscle (Figure 5C) of Mpc2$^{\Delta 16}$ mice compared to WT control mice. These data suggest that the Mpc2$^{\Delta 16}$ mice have normal sensitivity to the effects of insulin.

In contrast, Mpc2$^{\Delta 16}$ mice exhibited elevated blood lactate and trended toward a higher glucose AUC ($p=0.078$) during an intraperitoneal glucose tolerance test (GTT) (Figure 5D). Plasma insulin concentration was significantly lower in Mpc2$^{\Delta 16}$ mice compared to WT controls at baseline and 30 minutes after glucose injection (Figure 5E), suggesting that glucose intolerance in Mpc2$^{\Delta 16}$ mice was due to insufficient insulin secretion. Similarly, blood insulin concentration in Mpc2$^{\Delta 16}$ mice compared to WT controls was also significantly lower 15 minutes after a bolus pyruvate injection (Figure 4E).

Impaired glucose-stimulated insulin secretion in Mpc2$^{\Delta 16}$ mice is corrected by glibenclamide

The data obtained in GTT studies suggested a defect in glucose-stimulated insulin secretion (GSIS) by pancreatic islet beta cells of Mpc2$^{\Delta 16}$ mice. Both MPC1 and MPC2 are expressed in beta cells as demonstrated by colocalization with insulin in immunohistochemical staining of pancreatic sections (Figure 6A). Western blotting analyses confirmed that MPC1 and MPC2 proteins are expressed in isolated pancreatic islets and demonstrated that the expression of the MPC2$^{\Delta 16}$ protein was markedly reduced compared to WT MPC2 (Figure 6B). Islet insulin content in Mpc2$^{\Delta 16}$ mice was not different from WT controls (Figure 6C).

We examined GSIS in isolated pancreatic islets from WT and Mpc2$^{\Delta 16}$ mice. Compared to WT islets, Mpc2$^{\Delta 16}$ islets exhibited reduced insulin secretion in response to 23 mM glucose (Figure 6D). Beta cell glucose sensing requires mitochondrial pyruvate metabolism, resulting in closure of the K_{ATP} channels (Huopio et al., 2002). We therefore examined the effects of glibenclamide, a sulfonylurea drug that inhibits K channel activity, on GSIS in Mpc2$^{\Delta 16}$ ATP islets. As we hypothesized, the GSIS defect was rescued by the addition of glibenclamide to high-glucose media (Figure 6D). Additionally, Mpc2$^{\Delta 16}$ islets exhibited normal insulin secretion in response to KCl (Figure 6D). Supplementing high glucose medium with glutamine, a metabolic substrate that does not require the MPC complex to enter the mitochondrion to be oxidized, also corrected the defect in GSIS (Figure 6D). These findings collectively suggest that the Mpc2$^{\Delta 16}$ insulin secretion defect is specific to stimulation by mitochondrial pyruvate metabolism rather than a general deficiency in insulin production or defects in the insulin secretory machinery.

To confirm the relevance of these findings in vivo, we administered glibenclamide to Mpc2$^{\Delta 16}$ mice with a bolus of glucose in GTT studies. Vehicle-treated Mpc2$^{\Delta 16}$ mice exhibited elevated blood glucose concentration compared to WT mice at 30 and 60 min post-injection, but blood glucose concentrations in Mpc2$^{\Delta 16}$ mice treated with glibenclamide were not different compared to vehicle-treated WT mice (Figure 6E). Administration of glibenclamide did not affect plasma lactate concentration in mice of either genotype. Glibenclamide administration to Mpc2$^{\Delta 16}$ mice resulted in increased plasma insulin concentration, which was reduced in Mpc2$^{\Delta 16}$ mice versus WT mice, at 15 and 30 minutes after injection (Figure 6F). These data further support the model that whole body Mpc2-deficiency leads to a defect in GSIS that is improved by K_{ATP} channel inhibition.

DISCUSSION

Carrier-mediated transport of pyruvate across the inner mitochondrial membrane is a critical step in intermediary metabolism required for both anaplerotic and cataplerotic mitochondrial pyruvate metabolism. We found that complete loss of MPC2 leads to embryonic lethality, but that expression of a truncated MPC2 protein that exhibited hypomorphic activity was sufficient to support life. The most striking phenotypes of the Mpc2$^{\Delta 16}$ mice were elevated plasma lactate concentrations, particularly in the context of increased glucose concentrations, and a defect in beta cell GSIS leading to relative glucose intolerance. These findings are consistent with a function for MPC2 in regulating mitochondrial pyruvate utilization and reveal important roles for MPC2 in regulating whole body glucose homeostasis.

As mitochondrial pyruvate import is required in a number of critical metabolic pathways, it is not unexpected that complete ablation of Mpc2 resulted in embryonic lethality. Human mutations in MPC1 are associated with neonatal and juvenile mortality (Brivet, 2003). We were unable to recover viable Mpc2$^{-/-}$ embryos after day E11, just as mitochondrial function begins to play a larger role in embryonic metabolism (Cámara et al., 2011; Larsson et al., 1998; Metodiev et al., 2009; Park et al., 2007). Mpc2$^{+/-}$ mice exhibited only a modest reduction in MPC2 and MPC1 protein abundance and were phenotypically indistinguishable from WT littermates in every parameter we examined. Our inability to detect a phenotype from the Mpc2$^{+/-}$ mice, even under conditions of metabolic challenge, likely highlights an excess transport capacity of the MPC complex.

We also serendipitously created a truncated mutant MPC2 protein by virtue of the unpredictable results with zinc-finger nuclease mediated deletion. Despite having a nucleotide deletion larger than that of the Mpc2$^{-/-}$ (20 bp deletion compared to 2 bp deletion), the Mpc2$^{\Delta 16}$ mutant utilizes a down-stream methionine as an alternative start site for the translation of a truncated MPC2 protein. Since the original start codon is ablated by the 20 bp deletion, but is intact in the 2 bp deletion, this allows an alternative ribosomal entry sequence to be enforced. This start codon may be less efficient or the resulting protein less stable, since MPC2$^{\Delta 16}$ protein is less abundant than full length MPC2. Most tissues in the Mpc2$^{\Delta 16}$ mice also have a significant reduction in the abundance of the MPC1 protein. Previous work has shown that MPC1 and MPC2 must be coexpressed for proper assembly of the multimeric MPC complex and that depletion of either protein leads to reduced

abundance of the other (Bricker et al., 2012; Colca et al., 2013). It is likely that the reduced abundance of MPC1 in the Mpc2$^{\Delta 16}$ mice is due to lower quantity of Mpc2$^{\Delta 16}$ compared to WT protein. Diminished or weakened protein-protein interaction between the two proteins is also a potential factor in the reduced complex stability, since less MPC1 was co-immunoprecipitated with Mpc2$^{\Delta 16}$ compared to WT protein. However, the expression of MPC1 was only modestly affected by MPC2 truncation in BAT and islets, suggesting tissue-specific regulation of MPC complex stability or the possibility of homodimeric MPC protein complexes.

The truncated MPC2 protein is properly localized to the inner mitochondrial membrane and presumably, based on the phenotypes of the mutant mice, forming a transporter complex that is functionally hypomorphic. A number of mitochondrial carrier proteins of the IMM do not utilize canonical N-terminal mitochondrial localization sequences (Ferramosca and Zara, 2013; Pfanner and Geissler, 2001; Harbeuer et al., 2014). Instead, these carriers utilize internal sequences that that have yet to be defined. Indeed, analysis by mitochondrial localization prediction programs, which predict mitochondrial targeting based on these canonical N-terminal localization sequences, did not produce a high scoring prediction of mitochondrial localization for full length or Δ16 MPC2 protein. The focus of this paper was not to define the targeting sequence, since that has been elusive for most mitochondrial proteins that lack the N-terminal canonical sequence.

Since conversion of pyruvate into glucose by liver and kidney requires pyruvate to enter mitochondria for conversion to oxaloacetate, we expected that Mpc2$^{\Delta 16}$ mice might be hypoglycemic in conditions requiring gluconeogenesis. Previous work using isolated liver preparations and a chemical inhibitor of MPC activity showed an acute inhibition of hepatic glucose output (Martin-Requero et al., 1986; Rognstad, 1983; Thomas and Halestrap, 1981). However, whether carrier-mediated pyruvate transport by MPC has a significant control strength over gluconeogenesis has been debated (Groen et al., 1983, 1986; Halestrap and Armston, 1984) and the hypomorphic function of the MPC transport complex was not a limiting factor in the gluconeogenic capacity of Mpc2$^{\Delta 16}$ mice. Plasma ^{13}C-labeled glucose levels were actually increased in [U-^{13}C]PTT studies and Mpc2$^{\Delta 16}$ mice were not hypoglycemic following exhaustive exercise, suggesting that the Cori cycle was intact. The observation that gluconeogenesis is not impaired is not entirely unprecedented, given that previous studies have shown that up to 85% reduction in phosphoenolpyruvate carboxykinase expression does not impact gluconeogenic flux (Burgess et al., 2007). Further work with other, more complete, liver-specific loss-of-function models will be needed to define the role that MPC complex proteins play in regulating hepatic gluconeogenesis.

Another interesting phenotype of the Mpc2$^{\Delta 16}$ mice was the hyperglycemia detected during PTT and GTT studies. Since the insulin-stimulated decrease in blood glucose concentration was normal in ITT experiments, and pyruvate metabolism is important for beta cell glucose sensing (Lu et al., 2002; Prentki et al., 2013; Sugden and Holness, 2011), we suspected that insulin secretion might be defective. Indeed, plasma insulin concentration was diminished in Mpc2$^{\Delta 16}$ mice compared to WT mice during GTT and PTT studies, and isolated islets from Mpc2$^{\Delta 16}$ mice exhibited an attenuated insulin secretion response following the administration of 23 mM glucose. Glucose sensing and GSIS requires mitochondrial

pyruvate oxidation and carboxylation. Beta cells express very little lactate dehydrogenase and most of the pyruvate generated from glycolysis enters the mitochondrion for further metabolism (Malmgren et al., 2009; Schuit, 1997). Pyruvate carboxylation and oxidation inhibit ATP-sensitive potassium channels (K_{ATP}), depolarizing the beta cell membrane, opening voltage-dependent calcium channels, and triggering the release of insulin into circulation (Huopio et al., 2002). We found that the defects in insulin secretion by isolated islets and hypoinsulinemia/hyperglycemia in $Mpc2^{\Delta 16}$ mice were corrected by the sulfonylurea, glibenclamide, which functions by binding and inhibiting the regulatory subunit of K_{ATP} channels. It is likely that glibenclamide is able to circumvent the reduced capacity of $Mpc2^{\Delta 16}$ mutants for mitochondrial pyruvate metabolism. The observation that glutamine, which relies upon its own inner mitochondrial membrane carrier (Indiveri et al., 1998), is able to stimulate insulin secretion in $Mpc2^{\Delta 16}$ islets also supports a specific defect in mitochondrial pyruvate metabolism. Consistent with these data, while this paper was in review, Patterson and colleagues used chemical inhibitors and siRNA methods to suggest that MPC inhibition suppressed pyruvate metabolism and GSIS in isolated islets and beta cell lines (Patterson et al., 2014). Taken together, these studies demonstrate that the hypoinsulinemia of $Mpc2^{\Delta 16}$ mice is a specific defect in GSIS and not a broader indication of beta cell dysfunction.

The molecular identification of the MPC proteins has stimulated interest in targeting this complex for the treatment of many chronic disease states. Pharmacologic approaches to modulate the activity of the MPC complex could yield treatments for broad categories of obesity-related metabolic diseases, neurodegenerative conditions, and neoplastic diseases associated with impaired pyruvate metabolism (Constantin-Teodosiu, 2013; Schell and Rutter, 2013; Stacpoole, 2012). For example, the MPC complex has recently been identified as a binding site for the thiazolidinedione class of insulin sensitizers (Colca et al., 2013), which acutely modulate mitochondrial pyruvate oxidation (Divakaruni et al., 2013; Colca et al., 2013). The extent to which regulation of mitochondrial pyruvate import by thiazolidinediones affects insulin sensitization remains unclear, but could be addressed by MPC loss-of-function mouse models. Screens to identify small molecules that enhance, inhibit, or selectively modulate MPC activity may identify novel therapeutics with applicability to myriad chronic diseases.

EXPERIMENTAL PROCEDURES

Animal Studies

Unless otherwise noted, all experiments were conducted with 10-16 week old female mice generated and maintained in a pure C57BL/6 background. All animal experiments were approved by the Animal Studies Committee of Washington University School of Medicine.

Generation of Mpc2 Deficient Mice

The Mpc2 transgenic mice were generated by SAGE Labs using zinc-finger nuclease (ZFN) targeting technology (Geurts et al., 2009). Specifically, target site sequence, TCCCTAGGCCGCCGCGATggcagCTGCCGGCGCCCGAGGCC (NCBI Ref Seq:

NC_000067.5. Exon 1,nucleotides 199-203). ZFN pairs were microinjected into C57BL/6 zygotes and transferred to pseuodpregnant C57BL/6 females at 0.5 days post coitum.

Western Blotting

Polyacrylamide gel electrophoresis was performed on protein lysates utilizing Criterion precast gels (BioRad). Whole cell lysates from tissue or cell culture were collected in HNET buffer containing protease and phosphatase inhibitors. For blots of mitochondrial lysates, mitochondria were obtained by differential centrifugation and solubilized in HNET buffer containing protease and phosphatase inhibitors. Blots on isolated pancreatic islets involved isolation of islets as described below, and 50 islets solubilized in 5X LSB per lane. For immunoprecipitation 250 μg BAT mitochondrial lysate were solubilized in lysis buffer containing 0.2% NP-40 and 10% glycerol. Lysate was pre-cleared with 50 μL protein A beads, then incubated overnight with a rabbit MPC2 antibody (gift from Michael Wolfgang). 50 μL protein A beads were then added 1 hr prior to immunoprecipitation. Liver mitochondrial fractionation was conducted as previously (Benga et al., 1979) with slight modification. Briefly, digitonin treated mitochondria were centrifuged at 9500 × g. The digitonin supernatants were centrifuged at 100,000 × g to isolate the outer membrane pellet (OMM) and the supernatant containing the inner membrane space (IMS). The digitonin pellet was loaded onto a discontinuous sucrose gradient to generate mitoplasts. The mitoplasts were treated with Lubrol WX and the inner mitochondrial membrane (IMM) fractions were recovered from 100,000 × g discontinuous sucrose gradients. Antibodies utilized were: β-Actin (Sigma), Akt (Cell Signaling), pS473-Akt (Cell Signaling), CoxIV (Cell Signaling), cytochrome c (Abcam), lactate dehydrogenase (Abcam), MPC1 and MPC2 (gifts from Michael Wolfgang), pyruvate carboxylase (Santa Cruz), pyruvate dehydrogenase cocktail (Abcam), α-tubulin (Sigma), and VDAC (Abcam).

Quantitative PCR and RT-PCR

Total RNA was isolated using the RNAzol method (Tel-Test). Real-time PCR was performed using the ABI PRISM 7500 sequence detection system (Applied Biosystems, Foster City, CA) and the SYBR green kit. Arbitrary units of target mRNA were corrected by measuring the levels of 36B4 RNA. Sequence of the oligonucleotides used in qPCR analyses are listed in Supplemental Table 4.

Measurement of Mitochondrial Respiration

Mitochondria from heart and kidney were isolated by differential centrifugation. High resolution respirometry was conducted using a 2-chamber Oxygraph O2k (OROBOROS Instruments). 200 μg of mitochondria were added to 2 mL respiration buffer for each substrate trace. Respiratory substrates utilized were (concentration in mM): pyruvate (5)/ malate (2), methyl-pyruvate (20)/pyruvate (5)/malate (2), glutamate (10)/malate (2), and succinate (10) + 1 μM rotenone. During pyruvate stimulated respiration, 2 mM dichloroacetic acid was added to stimulate pyruvate dehydrogenase (Divakaruni et al., 2013). After substrate addition and measurement of basal respiration, maximally-stimulated, uncoupled respiration was measured by addition of 2 μg/mL oligomycin and 10 μM 2,4-dinitrophenol (DNP).

Isolation of Adult Murine Fibroblasts and Measurement of Mitochondrial Membrane Potential

Isolation of primary adult murine fibroblasts from tail clip was performed as previously described (Huss et al., 2004). Fibroblasts from WT and $Mpc2^{\Delta 16}$ mice were cultured in high-glucose DMEM supplemented with 20% fetal bovine serum. Cells were plated onto 4-well glass chamber slides (Lab-Tek II) at a density of 30,000 cells/well and incubated overnight. Cells were then stained with 100 nM tetramethylrhodamine, ethyl ester, perchlorate (TMRE) in HBSS for 30 min, washed with HBSS, and imaged on an inverted fluorescence microscope (Nikon Instruments Inc.). Average TMRE fluorescence per cell was determined with NIH ImageJ.

Acute Exercise Protocol

WT, $Mpc2^{\Delta 16}$, and $Mpc2^{+/-}$ mice performed a single bout of treadmill exercise to exhaustion. Mice were fasted for 4 hours prior to the exercise session. Following a 3 minute familiarization period on the treadmill, the exercise protocol consisted of graduated intensity running at 5 m/min for 5 min, 10 m/min for 5 minutes, 15 m/min for 10 minutes, 25 m/min for 15 minutes, and 30 m/min until the mouse fatigued. Mice were encouraged to run with a mild electric stimulus (20V) positioned at the end of the treadmill and were determined to be exhausted by their refusal to remain on treadmill belt for 5 seconds. Post-exercise blood glucose and lactate were collected at 0, 5, 10, 20, 30, 60, and 120 min after exhaustion.

Measurement of Baseline Plasma Parameters

Mice were fasted for 4-hours and tail blood glucose and lactate were determined using a One-Touch Ultra glucometer (LifeScan, Inc.) and a Lactate Plus lactate meter (Nova Biomedical), respectively. Blood samples for plasma analyses were collected by mandibular bleeding. Plasma insulin was measured with an ultra-sensitive ELISA (Crystal Chem). Plasma triglyceride and cholesterol were measured by Infinity assay kits (ThermoFisher). Non-esterified fatty acids (NEFA) and total ketones were measured using enzymatic assays (Wako Diagnostics).

Glucose, Pyruvate, and Insulin Tolerance Tests

For glucose and pyruvate tolerance tests, mice were fasted overnight for 16 hours and housed on aspen chip bedding. Mice were injected i.p. with 1 g/kg body weight glucose or with 2 g/kg body weight Na-pyruvate dissolved in sterile physiological saline. For the insulin tolerance test, mice were fasted for 6 hours and injected i.p. with 0.75 U/kg body weight insulin. Tail blood glucose and lactate were determined at 0, 30, 60, and 120 minute after challenge as described above. Total area under the curve was calculated using the trapezoidal rule. Blood samples for plasma insulin quantification were collected by mandibular bleeding as described above. A subset of mice were injected i.p. with 2 g/kg body weight Na-pyruvate and sacrificed at 15 minutes to determine plasma insulin during pyruvate challenge. To examine insulin-stimulated protein phosphorylation, a subset of mice were injected i.p. with 10 mU/g body weight human insulin 15 minutes before sacrifice to collect liver and muscle tissue.

The glibenclamide rescue studies were conducted in the context of a standard GTT, with sample time points adjusted to 0, 15, 30, and 60 minute after challenge. Glibenclamide was administered at 0.1 mg/kg body weight in a glucose solution that contained 0.1% DMSO. Blood was collected at each time point by means of mandibular bleeding as described above.

^{13}C-Labled Pyruvate Studies

Pyruvate labeling studies were conducted as previously described (Méndez-Lucas et al., 2013). Briefly, mice were fasted for 16 hours and injected i.p. with 2 g pyruvate per kg body weight with a 10% enrichment of uniformly labeled [U-^{13}C3]Napyruvate (Cambridge Isotope Laboratories), Inc. Mice were sacrificed 60 minutes post-injection and plasma was analyzed by GC-MS as previously described (Sunny and Bequette, 2010).

Pancreas immunohistochemistry

Protein expression of MPCs in pancreatic islets was determined in paraffin-embedded pancreatic sections from WT mice cut onto glass slides. Slides were rehydrated, permeabilized with trypsin, blocked in 1% BSA, and probed with either rabbit anti-MPC1 or rabbit anti-MPC2 (gifts from Michael Wolfgang) in addition to guinea pig anti-insulin (Abcam), all 1:200 in 1% BSA overnight. Sections were then washed 3 times for 5 min in PBS and probed with 1:1000 donkey anti-rabbit green or 1:1000 donkey anti-guinea pig red Alexa Fluor secondary antibodies (Invitrogen) for 2 hours. Slides were again washed 3 times for 5 min in PBS, mounted with Vectashield + DAPI, and imaged on an epifluorescence microscope (Nikon Instruments Inc.).

Islet isolation and insulin release experiments

Islet isolation and insulin release studies were performed as previously described (Remedi et al., 2004). Briefly, following euthanization, pancreases were removed and injected with Hank's balanced salt solution (Sigma, St. Louis, MO) containing collagenase (0.5 mg/ml; pH 7.4), digested for 4 min at 37°C, and the islets isolated by hand. Following overnight incubation in 3 mM glucose CMRL-1066 medium, islets (10 per well in 12 well plates) were incubated for 60 min at 37°C in CMRL-1066 plus 1 mM glucose, 23 mM glucose, 23 mM glucose + 1 μM glibenclamide, 1 mM + 30 mM KCl, or 23 mM glucose + 10 mM glutamine, as indicated. After the incubation period, the medium was removed and assayed for insulin release. Experiments were repeated in triplicate. For islet insulin content, groups of 10 islets were disrupted using ethanol-HCl extraction and sonicated on ice for estimation of insulin content. Insulin secretion and content were measured using a Rat Insulin radioimmunoassay according to manufacturer's procedure (Millipore).

Statistical Analyses

Statistical comparisons were made using analysis of variance (ANOVA), chi-squared test, or *t*-test. All data are presented as means ± SEM, with a statistically significant difference defined as a P value <0.05.

Supplementary Material

Refer to Web version on PubMed Central for supplementary material.

Acknowledgments

This work was supported by NIH grants R01 DK078187 and R42 AA021228. A grant from the Barnes Jewish Hospital Foundation and the core services of the Digestive Diseases Research Core Center (P30 DK52574), Diabetes Research Center (P30 DK20579) and the Nutrition Obesity Research Center (P30 DK56341) at Washington University School of Medicine also supported this work. S.C.B. is supported by NIH grants P01 DK078184, P01 DK058398, and the Robert A. Welch Foundation (I-1804-01). P.A.V. and K.S.M are Diabetes Research Postdoctoral Training Program fellows (T32 DK007296). G.G.S. is supported by NIH training grant T32 HL007275 and K.T.C. is an American Liver Foundation Liver Scholar. We wish to disclose that authors Cole, McDonald, Colca, and Kletzien are founders, employees, and significant stockholders of Metabolic Solutions Development Co.

References

Benga G, Hodarnau A, Tilinca R, Porutiu D, Dancea S, Pop V, Wrigglesworthf J. Fractionation of Human Liver Mitochondria: Enzymic and Morphological Characterization of the Inner and Outer Membranes as Compared to Rat Liver Mitochondria. J. Cell Sci. 1979; 429:417–429. [PubMed: 422680]

Bricker DK, Taylor EB, Schell JC, Orsak T, Boutron A, Chen Y-C, Cox JE, Cardon CM, Van Vranken JG, Dephoure N, et al. A mitochondrial pyruvate carrier required for pyruvate uptake in yeast, Drosophila, and humans. Science. 2012; 337:96–100. [PubMed: 22628558]

Brivet M, Garcia-Cazorla A, Lyonnet S, Dumez Y, Nassogne MC, Slama A, Boutron A, Touati G, Legrand A, Saudubray JM. Impaired mitochondrial pyruvate importation in a patient and a fetus at risk. Mol. Genet. Metab. 2003; 78:186–192. [PubMed: 12649063]

Burgess SC, He T, Yan Z, Lindner J, Sherry a D. Malloy CR, Browning JD, Magnuson M. a. Cytosolic phosphoenolpyruvate carboxykinase does not solely control the rate of hepatic gluconeogenesis in the intact mouse liver. Cell Metab. 2007; 5:313–320. [PubMed: 17403375]

Cámara Y, Asin-Cayuela J, Park CB, Metodiev MD, Shi Y, Ruzzenente B, Kukat C, Habermann B, Wibom R, Hultenby K, et al. MTERF4 regulates translation by targeting the methyltransferase NSUN4 to the mammalian mitochondrial ribosome. Cell Metab. 2011; 13:527–539. [PubMed: 21531335]

Colca JR, McDonald WG, Cavey GS, Cole SL, Holewa DD, Brightwell-Conrad AS, Wolfe CL, Wheeler JS, Coulter KR, Kilkuskie PM, et al. Identification of a mitochondrial target of thiazolidinedione insulin sensitizers (mTOT)--relationship to newly identified mitochondrial pyruvate carrier proteins. PLoS One. 2013; 8:e61551. [PubMed: 23690925]

Constantin-Teodosiu D. Regulation of Muscle Pyruvate Dehydrogenase Complex in Insulin Resistance: Effects of Exercise and Dichloroacetate. Diabetes Metab. J. 2013; 37:301–314. [PubMed: 24199158]

Divakaruni AS, Wiley SE, Rogers GW, Andreyev AY, Petrosyan S, Loviscach M, Wall E. a, Yadava N, Heuck AP, Ferrick D. a, et al. Thiazolidinediones are acute, specific inhibitors of the mitochondrial pyruvate carrier. Proc. Natl. Acad. Sci. U. S. A. 2013; 110:5422–5427. [PubMed: 23513224]

Ferramosca A, Zara V. Biogenesis of mitochondrial carrier proteins: molecular mechanisms of import into mitochondria. Biochim. Biophys. Acta. 2013; 1833:494–502. [PubMed: 23201437]

Geurts AM, Cost GJ, Freyvert Y, Zeitler B, Miller JC, Choi VM, Jenkins SS, Wood A, Cui X, Meng X, et al. Knockout rats via embryo microinjection of zinc-finger nucleases. Science. 2009; 325:433. [PubMed: 19628861]

Groen AK, Vervoorn RC, Van der Meer R, Tager M. Control of Gluconeogenesis in Rat Liver Cells. J. Biol. Chem. 1983; 258:14346–14353. [PubMed: 6643485]

Groen K, van Roermund WT, Vervoorn C, Tager M. Control of gluconeogenesis in rat liver cells. Biochem. J. 1986; 237:379–389. [PubMed: 3800895]

Halestrap AP. The Mitochondrial Pyruvate Carrier. Biochem. J. 1975; 148:85–96. [PubMed: 1156402]

Halestrap, a P.; Armston, a E. A re-evaluation of the role of mitochondrial pyruvate transport in the hormonal control of rat liver mitochondrial pyruvate metabolism. Biochem. J. 1984; 223:677–685. [PubMed: 6095807]

Halestrap AP, Denton RM. The specificity and metabolic implications of the inhibition of pyruvate transport in isolated mitochondria and intact tissue preparations by alpha-Cyano-4-hydroxycinnamate and related compounds. Biochem. J. 1975; 148:97–106. [PubMed: 1171687]

Harbauer AB, Zahedi RP, Sickmann A, Pfanner N, Meisinger C. The Protein Import Machinery of Mitochondria-A Regulatory Hub in Metabolism, Stress, and Disease. Cell Metab. 2014; 19:357–372. [PubMed: 24561263]

Herzig S, Raemy E, Montessuit S, Veuthey J-L, Zamboni N, Westermann B, Kunji ERS, Martinou J-C. Identification and functional expression of the mitochondrial pyruvate carrier. Science. 2012; 337:93–96. [PubMed: 22628554]

Huopio H, Shyng S-L, Otonkoski T, Nichols CG. K(ATP) channels and insulin secretion disorders. Am. J. Physiol. Endocrinol. Metab. 2002; 283:E207–16. [PubMed: 12110524]

Huss JM, Torra IP, Staels B, Kelly DP, Torra P, Gigue V. Estrogen-Related Receptor α Directs Peroxisome Proliferator-Activated Receptor α Signaling in the Transcriptional Control of Energy Metabolism in Cardiac and Skeletal Muscle. Mol. Cell. Biol. 2004; 24:9079–9091. [PubMed: 15456881]

Indiveri C, Abruzzo G, Stipani I, Palmieri F. Identification and purification of the reconstitutively active glutamine carrier from rat kidney mitochondria. Biochem. J. 1998; 333:285–290. [PubMed: 9657967]

Jensen MV, Joseph JW, Ronnebaum SM, Burgess SC, Sherry AD, Newgard CB. Metabolic cycling in control of glucose-stimulated insulin secretion. 2008; 27704:1287–1297.

Katz J, Tayek JA. Recycling of glucose and determination of the Cori Cycle and gluconeogenesis. Am. J. Physiol. - Endocrinol. Metab. 1999; 277:401–407.

Larsson NG, Wang J, Wilhelmsson H, Oldfors A, Rustin P, Lewandoski M, Barsh GS, Clayton DA. Mitochondrial transcription factor A is necessary for mtDNA maintenance and embryogenesis in mice. Nat. Genet. 1998; 18:231–236. [PubMed: 9500544]

Lu D, Mulder H, Zhao P, Burgess SC, Jensen M. V, Kamzolova, S. Newgard CB, Sherry a D. 13C NMR isotopomer analysis reveals a connection between pyruvate cycling and glucose-stimulated insulin secretion (GSIS). Proc. Natl. Acad. Sci. U. S. A. 2002; 99:2708–2713. [PubMed: 11880625]

Malmgren S, Nicholls DG, Taneera J, Bacos K, Koeck T, Tamaddon A, Wibom R, Groop L, Ling C, Mulder H, et al. Tight coupling between glucose and mitochondrial metabolism in clonal beta-cells is required for robust insulin secretion. J. Biol. Chem. 2009; 284:32395–32404. [PubMed: 19797055]

Martin-Requero A, Ayuso MS, Parrillas R. Rate-limiting Steps for Hepatic Gluconeogenesis. J. Biol. Chem. 1986; 261:13973–13978. [PubMed: 3771515]

Méndez-Lucas A, Duarte JAG, Sunny NE, Satapati S, He T, Fu X, Bermúdez J, Burgess SC, Perales JC. PEPCK-M expression in mouse liver potentiates, not replaces, PEPCK-C mediated gluconeogenesis. J. Hepatol. 2013; 59:105–113. [PubMed: 23466304]

Metodiev MD, Lesko N, Park CB, Cámara Y, Shi Y, Wibom R, Hultenby K, Gustafsson CM, Larsson N-G. Methylation of 12S rRNA is necessary for in vivo stability of the small subunit of the mammalian mitochondrial ribosome. Cell Metab. 2009; 9:386–397. [PubMed: 19356719]

Papa S, Francavilla A, Paradies G, Meduri B. The Transport of Pyruvate in Rat Liver Mitochondria. FEBS Lett. 1971; 12:285–288. [PubMed: 11945601]

Park CB, Asin-Cayuela J, Cámara Y, Shi Y, Pellegrini M, Gaspari M, Wibom R, Hultenby K, Erdjument-Bromage H, Tempst P, et al. MTERF3 is a negative regulator of mammalian mtDNA transcription. Cell. 2007; 130:273–285. [PubMed: 17662942]

Patterson JN, Cousteils K, Lou JW, Manning Fox JE, Macdonald PE, Joseph JW. Mitochondrial metabolism of pyruvate is essential for regulating glucose-stimulated insulin secretion. J. Biol. Chem. 2014 DOI: 10.1074/jbc.M113.521666.

Pfanner N, Geissler A. Versatility of the mitochondrial protein import machinery. Nat. Rev. Mol. Cell Biol. 2001; 2:339–349. [PubMed: 11331908]

Pilkis SJ, R E-MM, H CT. Hormonal regulation of hepatic gluconeogenesis and glycolysis. Annu. Rev. Biochem. 1988; 57:755–783. [PubMed: 3052289]

Prentki M, Matschinsky FM, Madiraju SRM. Metabolic signaling in fuel-induced insulin secretion. Cell Metab. 2013; 18:162–185. [PubMed: 23791483]

Remedi MS, Koster JC, Markova K, Seino S, Miki T, Patton BL, McDaniel ML, Nichols CG. Diet-induced glucose intolerance in mice with decreased beta-cell ATP-sensitive K+ channels. Diabetes. 2004; 53:3159–3167. [PubMed: 15561946]

Rognstad R. The Role of Mitochondrial Pyruvate Transport in the Control of Lactate Gluconeogenesis. Int. J. Biochem. 1983; 15:1417–1421. [PubMed: 6653863]

Schell JC, Rutter J. The long and winding road to the mitochondrial pyruvate carrier. Cancer Metab. 2013; 1:6. [PubMed: 24280073]

Schuit F. Metabolic Fate of Glucose in Purified Islet Cells. Glucose-Regulated Anaplerosis in Beta Cells. J. Biol. Chem. 1997; 272:18572–18579. [PubMed: 9228023]

Stacpoole PW. The pyruvate dehydrogenase complex as a therapeutic target for age-related diseases. Aging Cell. 2012; 11:371–377. [PubMed: 22321732]

Sugden MC, Holness MJ. The pyruvate carboxylase-pyruvate dehydrogenase axis in islet pyruvate metabolism: Going round in circles? Islets. 2011; 3:302–319. [PubMed: 21934355]

Sunny NE, Bequette BJ. Gluconeogenesis differs in developing chick embryos derived from small compared with typical size broiler breeder eggs. J. Anim. Sci. 2010; 88:912–921. [PubMed: 19966165]

Thomas AP, Halestrap AP. The role of mitochondrial pyruvate transport in the stimulation by glucagon and phenylephrine of gluconeogenesis from L-lactate in isolated rat hepatocytes. Biochem. J. 1981; 198:551–560. [PubMed: 7326022]

Highlights

- Complete MPC2 deficiency in mice is lethal in utero.
- Mice expressing an N-terminus truncated, hypomorphic MPC2 protein are viable.
- MPC2 hypomorphism increased lactate levels, but did not affect gluconeogenesis.
- Glucose-stimulated insulin secretion is impaired in MPC2 hypomorphic mice.

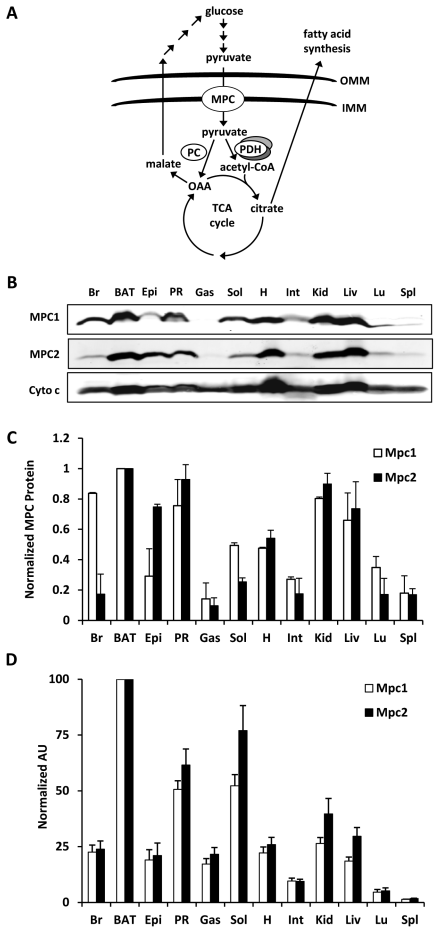

Figure 1. MPC proteins are highly expressed in tissues with high mitochondrial content

(A) The schematic depicts an overview of mitochondrial pyruvate metabolism. Abbreviations: outer mitochondrial membrane (OMM), inner MM (IMM), pyruvate carboxylase (PC), pyruvate dehydrogenase (PDH), oxaloacetate (OAA), and tricarboxylic acid (TCA). **(B)** Western blot depicting expression of the indicated proteins in whole cell lysates from various C57Bl/6 mouse tissues. Cytochrome c (cyto c) is shown to demonstrate mitochondrial abundance in the whole cell lysates. **(C)** Quantified densitometry of western blot shown in (B). Data are presented as mean ± SEM (n=3 separate animals). **(D)** Expression pattern of Mpc1 and Mpc2 in C57Bl/6 mice as measured by qRT-PCR. Values are expressed as arbitrary units (AU) and presented as mean ± SEM (n=5 separate animals). Abbreviations: brain (Br), brown adipose tissue (BAT), epididymal adipose tissue (Epi), perirenal adipose tissue (PR), gastrocnemius (Gas), soleus (Sol), heart (H), intestine (Int), kidney (Kid), liver (Liv), lung (Lu), and spleen (Spl).

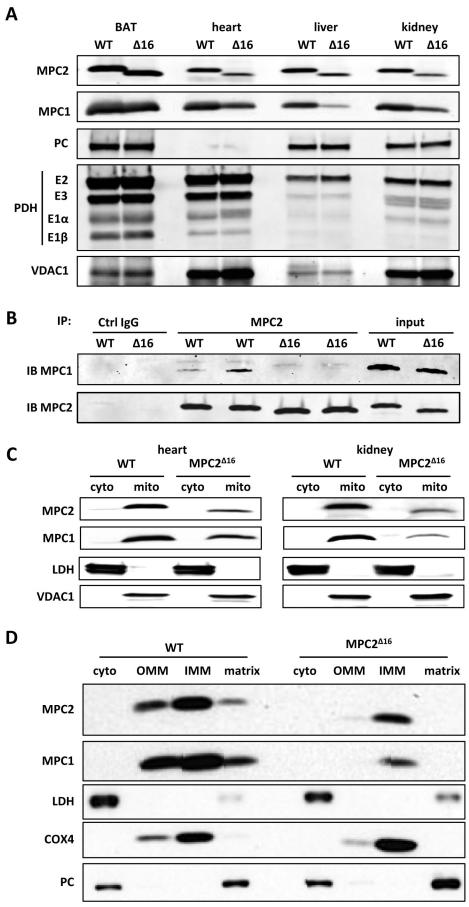

Figure 2. Generation of MPC2 deficient mice

(A) Western blot depicting the abundance of MPC1, MPC2, pyruvate carboxylase (PC), and pyruvate dehydrogenase complex (PDH) protein in mitochondrial lysates of various tissues from Mpc2$^{\Delta 16}$ mice and WT controls. Voltage-dependent anion channel-1 (VDAC1) is used as a loading control. **(B)** The ability of WT MPC2 and MPC2$^{\Delta 16}$ protein to co-immunoprecipitate MPC1 was tested by using an antibody against the C-terminus of MPC2 and BAT mitochondrial lysates from WT and Mpc2$^{\Delta 16}$ mice. Negative control (irrelevant IgG) and input (non-precipitated mitochondrial lysates) are also shown for comparison. **(C)** Western blots for MPC1 and MPC2 after sub-cellular fractionation to separate cytosolic and mitochondrial fractions from WT and Mpc2$^{\Delta 16}$ mice are shown. Lactate dehydrogenase (LDH) is used to demarcate the cytosolic fraction while VDAC1 demarcates the mitochondrial fraction. **(D)** Western blots after mitochondrial sub-fractionation to separate cytosolic, OMM, IMM, and matrix components by using liver from WT and Mpc2$^{\Delta 16}$ mice. LDH demarcates the cytosolic fraction, cytochrome c oxidase subunit 4 (Cox4) demarcates the IMM, and PC demarcates the matrix.

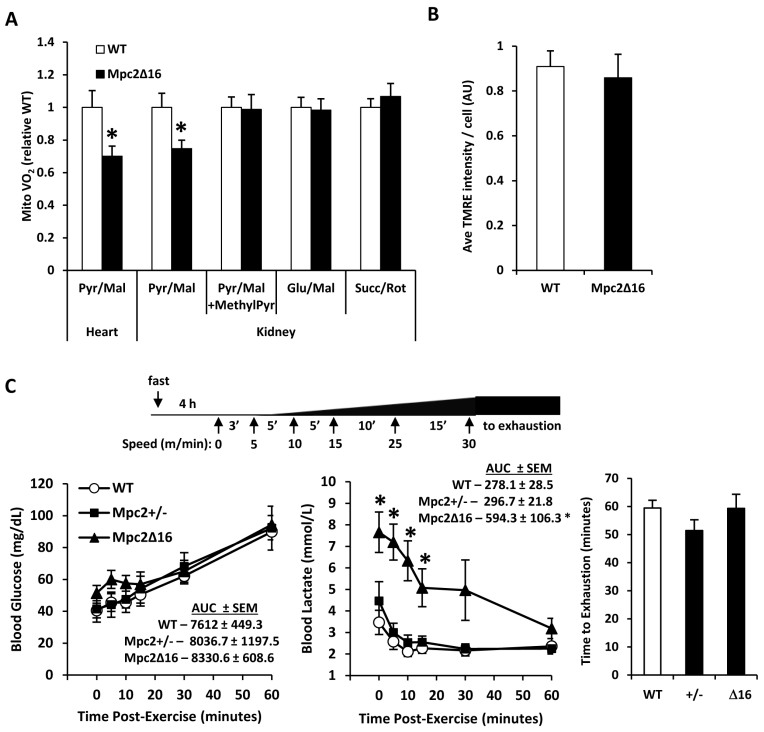

Figure 3. Mpc2$^{\Delta 16}$ mice have diminished capacity for pyruvate utilization, but exercise capacity is unimpaired

(A) DNP-stimulated rates of oxygen consumption by mitochondria isolated from heart or kidney of WT or Mpc2$^{\Delta 16}$ mice in the presence of the indicated substrates (n=8). **(B)** TMRE staining of tail fibroblasts isolated from WT or Mpc2$^{\Delta 16}$ mice (n=8, separate experiments in duplicate). **(C)** Schematic of exercise protocol is shown. Blood glucose and blood lactate curves for WT, Mpc2$^{+/-}$, and Mpc2$^{\Delta 16}$ mice following graduated-intensity exercise on a motor-driven treadmill (n=6). Elapsed time until exhaustion for WT, Mpc2$^{+/-}$, and Mpc2$^{\Delta 16}$ mice during graduated-intensity exercise (n=6). Data are presented as mean ± SEM. *P < 0.05, **P < 0.01 Mpc2$^{\Delta 16}$ versus WT.

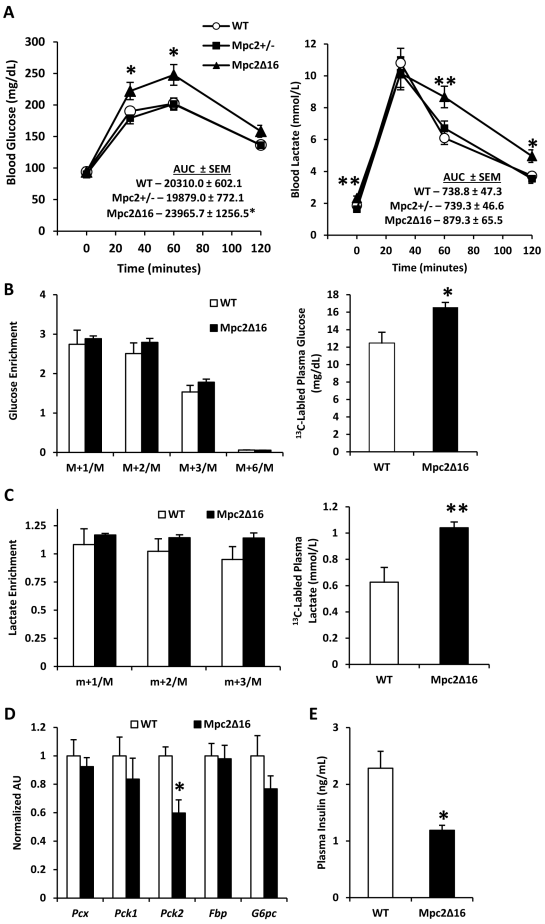

Figure 4. Mpc2$^{\Delta 16}$ mice have elevated blood glucose and blood lactate during a pyruvate tolerance test, but gluconeogenesis remains unimpaired

(A) Blood glucose and blood lactate curves for WT, Mpc2$^{+/-}$, and Mpc2$^{\Delta 16}$ mice during i.p. pyruvate tolerance test (n=14). **(B)** ^{13}C enrichment of plasma glucose isotopomers and total ^{13}C-labled plasma glucose, **(C)** ^{13}C enrichment of plasma lactate isotopomers and total ^{13}C-labled plasma lactate (n=7). Data are presented as mean ± SEM. *P < 0.05, **P < 0.01 Mpc2$^{\Delta 16}$ versus WT. **(D)** Expression of liver gluconeogenesis enzymes. **(E)** Plasma insulin 15 minutes post bolus pyruvate injection.

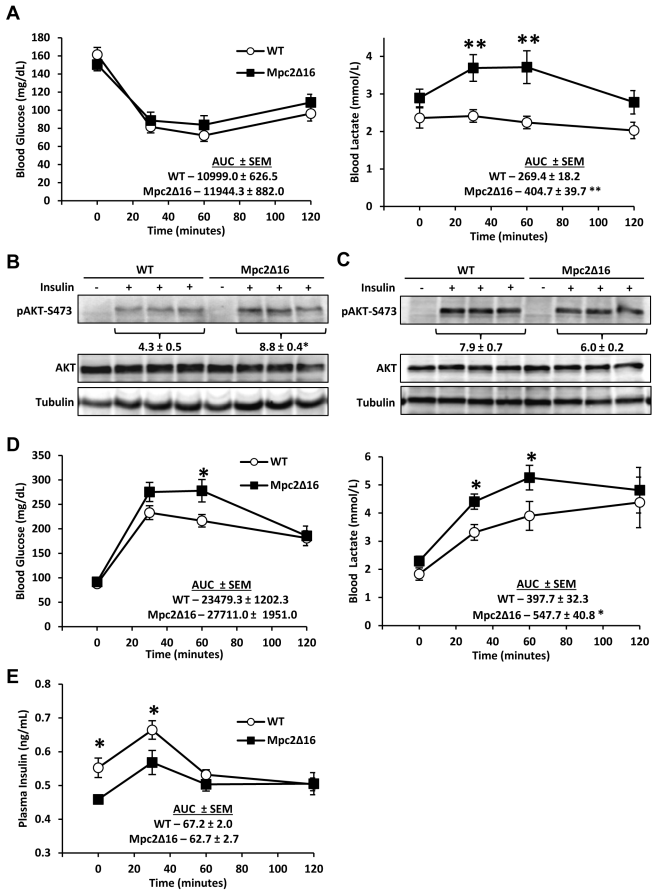

Figure 5. Mpc2$^{\Delta 16}$ mice are responsive to insulin, but are glucose intolerant and hypoinsulinemic

(A) Blood glucose and blood lactate curves for WT and Mpc2$^{\Delta 16}$ mice during i.p. insulin tolerance test (n=14). Data are presented as mean ± SEM. *P < 0.05, **P < 0.01 Mpc2$^{\Delta 16}$ versus WT. **(B)** Western blot and quantified densitometry of liver S473-AKT phosphorylation 15 minutes post insulin injection. **(C)** Western blot and quantified densitometry of gastroc S473-AKT phosphorylation 15 minutes post insulin injection. **(D)** Blood glucose and blood lactate curves for WT and Mpc2$^{\Delta 16}$ mice during an i.p. glucose tolerance test (n=15). **(E)** Plasma insulin from blood collected during an i.p. glucose challenge (n=9). Data are presented as mean ± SEM. *P < 0.05, **P < 0.01 Mpc2$^{\Delta 16}$ versus WT.

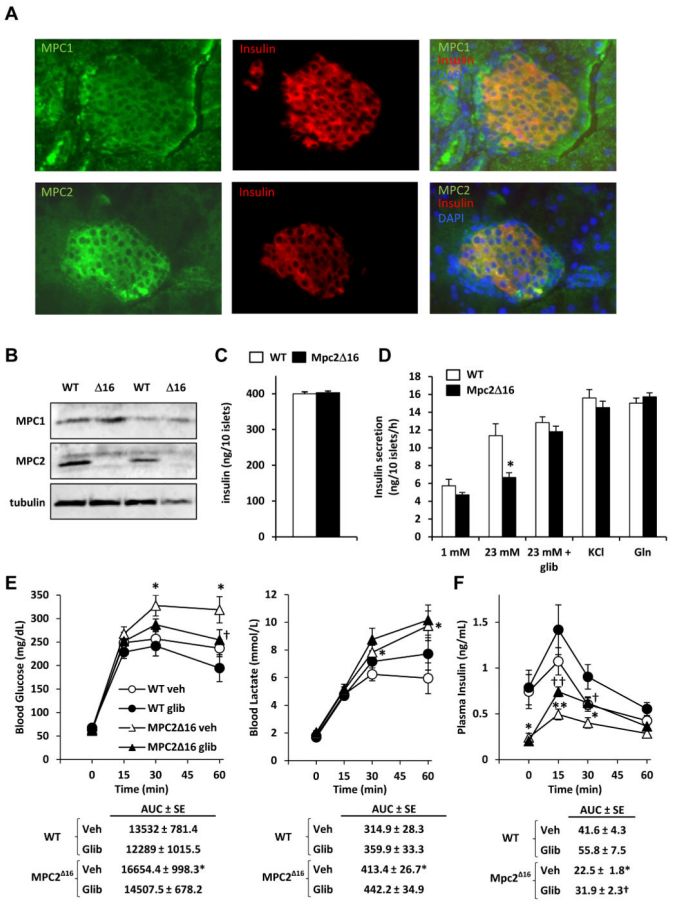

Figure 6. Elevated blood glucose and defective GSIS in Mpc2$^{\Delta 16}$ mice are corrected by glibenclamide treatment

(A) Images from immunofluorescent staining of pancreatic islets from C57Bl/6 mice with antibodies against MPC1 (green), MPC2 (green), or insulin (red) are shown. **(B)** Western blot depicting the abundance of MPC2 and MPC1 protein using protein lysates from isolated islets from Mpc2$^{\Delta 16}$ mice and WT controls. **(C)** Insulin content of islets isolated from WT and Mpc2$^{\Delta 16}$ mice (n=6). **(D)** Insulin secretion by isolated pancreatic islets from WT and Mpc2$^{\Delta 16}$ mice in response to the indicated stimuli (n=6). **(E)** Blood glucose and blood lactate curves during an i.p. glucose tolerance test for WT and Mpc2$^{\Delta 16}$ mice treated with glibenclamide or saline vehicle (n=11-13). **(F)** Plasma insulin from blood collected during the experiment described in E (n=11-13). Data are presented as mean ± SEM. *P < 0.05, **P < 0.01 Mpc2$^{\Delta 16}$ versus WT.

Table 1

Baseline plasma parameters

	WT	MPC2Δ16
Glucose (mg/dL)	125.1 ± 5.7	124.3 ± 5.1
Lactate (mmol/L)	1.6 ± 0.09	2.3 ± 0.11*
Insulin (ng/mL)	0.51 ± 0.09	0.34 ± 0.03
TG (mg/dL)	61.8 ± 2.2	54.8 ± 1.9*
NEFA (mmol/L)	0.58 ± 0.05	0.67 ± 0.05
Cholesterol (mg/dL)	65.3 ± 2.6	58.3 ± 3.7
Total Ketones (mmol/L)	0.15 ± 0.01	0.25 ± 0.01*

* $p<0.05$ versus WT.